Electronic Supplementary Information

Arrested Mesoscopic Growth of Toroidal Nanoobjects by Molecular Control of Interaction Surfaces

Ryuichi Kawai,[a] Yuhei Yamada,[a] Sougata Datta,[b] Hiroki Hanayama[c] and Shiki Yagai[*b,c]

a. Division of Advanced Science and Engineering, Graduate School of Engineering, Chiba University, 1-33 Yayoi-cho, Inage-ku, Chiba 263-8522, Japan.
b. Institute for Advanced Academic Research (IAAR), Chiba University, 1-33 Yayoi-cho, Inage-ku, Chiba 263-8522, Japan.
c. Department of Applied Chemistry and Biotechnology, Graduate School of Engineering, Chiba University, 1-33 Yayoi-cho, Inage-ku, Chiba 263-8522, Japan.

E-mail: yagai@faculty.chiba-u.jp
Fax: +81-(0)43-290-3401
Tel: +81-(0)43-290-3169

Table of Contents

1. General

Materials and methods:

All starting materials and reagents, purchased from commercial suppliers, were of reagent grade and used without further purification. Medium-pressure column chromatography was carried out with a Biotage Flash Purification System Isoler™ One using Biotage® Sfär Silica High Capacity Duo 20 μm 25 g cartridges. The solvents used for the preparation of supramolecular assemblies and measurements were either spectroscopic grade or solvents with a purity of at least 95.0%, which were used as received without further purification. Gel permeation chromatography (GPC) was performed with recycling preparative liquid chromatography (LC-9225NEXT, Japan Analytical Industry) equipped with two GPC columns (JAIGEL-2HR Plus and JAIGEL-2.5HR Plus). ^{1}H and ^{13}C nuclear magnetic resonance (NMR) spectra were recorded in $CDCl_3$ at 293 K on a Bruker AVANCE III-500M NMR spectrometers. Chemical shifts were reported in parts per million (ppm, δ) and were referenced to the signals of tetramethylsilane (TMS) at 0.00 ppm as internal standard. The resonance multiplicity is described as s (singlet), d (doublet), t (triplet), and m (multiplet). In the proton assignments, "Anth" denotes the anthracene ring. High-resolution mass spectra (HRMS) were measured on an Exactive (Thermo Scientific) using electrospray ionization (ESI). Ultraviolet/visible (UV/Vis) absorption spectra were recorded on a JASCO V760 spectrophotometer equipped with a JASCO ETCS-761 temperature-control unit. Circular dichroism (CD) spectra were recorded on a JASCO J820 spectropolarimeter equipped with a JASCO PTC-423L temperature controller unit. Fluorescent spectra were recorded on a JASCO FP-8300 spectrofluorometer equipped with a JASCO-815 temperature controller. These spectra were recorded using a screw-capped quartz cuvette of 1.0 mm or 10 mm pathlength. Molecular mechanics calculations were performed on MacroModel/Maestro version 12.2 (Schrödinger) with OPLS2005 force field without solvent.

Atomic force microscopy (AFM):

AFM images were obtained under ambient conditions using a Multimode 8 Nanoscope V (Bruker AXS) in Peak Force Tapping (ScanAsyst) mode. The scan rate was set to 0.996 Hz. Silicon cantilevers (SCANASYST-AIR) with a spring constant of 0.4 N/m and a frequency of 70 kHz (nominal value, Bruker, Japan) were used. The samples were prepared by spin-coating (3000 rpm, 1 min) approximately 10 μL of MCH solutions of assemblies onto freshly cleaved highly oriented pyrolytic graphite (HOPG, 0.5 cm × 0.5 cm) at room temperature. AFM images were processed using NanoScope Analysis 3.0 (Bruker).

All-atom molecular dynamics simulation:

All-atom molecular dynamics (AA-MD) simulations of self-assembled **2** were performed in methylcyclohexane (MCH) using GROMACS 2025.4.[S1] Intra- and intermolecular interactions were described using the General Amber Force Field (GAFF).[S2] The partial atomic charges of **2** and MCH were obtained by applying the restrained electrostatic potential (RESP) method, based on quantum chemical calculations at the HF/6-31G(d) level with the Gaussian 16 program package.[S3] The initial self-assembled structure was composed of 10 molecules of **2**, in which π-conjugated units were stacked, and the hydrogen-bonding units were connected, and the space in the simulation box was filled with MCH. Initial box dimensions were 6.0 × 6.0 × 13.0 nm^3. Pre-equilibration runs under constraints applied to intermolecular hydrogen bonds were performed for 10 ns at 300 K and 1 bar of temperature and pressure, respectively, coupling using the v-rescale thermostat and c-rescale barostat. After removal of these constraints, production runs were performed for 110 ns under the same conditions. The time step was set to 2 fs and all covalent bonds connected to hydrogen atoms were constrained by using the LINCS algorithm.[S4]

Small-angle X-ray scattering (SAXS) measurements and analysis:

SAXS measurements were conducted at BL-10C at the Photon Factory of the High Energy Accelerator Research Organization (KEK) in Tsukuba, Japan. Sample solutions were placed in specialized cells featuring a stainless-steel frame and 20-μm-thick quartz glass windows, with a 1.25-mm optical path length. Temperature was maintained at room temperature. The experimental setup using X-ray wavelength of 1.5 Å and a sample-detector distance of 1029 mm (calibrated using silver behenate) allowed for a detectable Q-range spanning from 0.1 to 5.9 nm^{-1}. Data were collected in 60 frames, each with an exposure time of 10 s. No signs of radiation damage were observed, allowing the frames to be averaged, resulting in a total integration time of 600 s. Scattering data were captured using a DECTRIS PILATUS3 2M detector and subsequently converted from 2D to 1D scattering intensity profiles [$I(Q)$ versus Q] through radial averaging. The resulting intensity data were normalized with water as a reference standard. The background, attributed to both solvent and cell, was subtracted to yield absolute scattering intensities, reported as $I(Q)$ in cm^{-1}. All data reduction were executed using the SAngler software package.[S5] In temperature-dependent SAXS experiments, the temperature of sample solution was controlled using a HCS302-LN190 (Instec Inc.). Sample solutions were placed in quartz capillaries (2 mm in diameter and 10 μm in wall thickness), and the top

of the capillary was sealed with resin to avoid evaporation of the solvent at higher temperature. SAXS data were collected using X-ray with a wavelength of 1 Å.

Analysis of SAXS data:

The fitting approaches were carried out using SasView (http://www.sasview.org/) using the core plus three shell cylinder model.[S6] The core is comprised of solvent, and the three shells are (1) the branch alkyl chains, (2) the aromatic unit, and (3) long *n*-$C_{12}H_{25}$ side chains. An additional Lorentzian peak function[S7] was used to describe the peak arising from the stacking of two toroids. The scattered intensity of the core-three shell cylinder adding Lorentzian peak function is calculated using following equation:

$$I_{(q,\alpha)} = \frac{scale}{V_{total}} F^2(q,\alpha)\sin(\alpha) + I_{peak} + I_{bkg} \quad \text{(S1)}$$

In the above, "scale" is the (known) volume fraction, α is the angle between the cylinder axis and the scattering vector, q. V_{total} is the total cylinder volume, including shells and the scale is related to the volume fraction. F(q,α) is given as follows:

$$F(q,a) = \sum_{k=0}^{3}\left[(\rho_k - \rho_{k+1})V_k \frac{\sin\left({}^1/_2\, L.q.\cos\alpha\right)}{{}^1/_2\, L.q.\cos\alpha}\frac{2J_1(q.r_k\sin\alpha)}{q.r_k\sin\alpha}\right] exp\left\{-\frac{1}{2}q^2\sigma^2\right\} \quad \text{(S2)}$$

In the equation S2, $V_{\text{k}} = \pi L_{\text{core}} r_{\text{k}}^2$ is the volume of each shell k, with $r_{\text{k}} = r_{\text{k-1}} + l_{\text{k}}$, where $r_{\text{k=0}} = r_{\text{core}}$ (core radius). The parameters l_{k} and ρ_{k} are the thicknesses and scattering length densities of shell k. The core radius lies when $k = 0$. The Lorentzian peak function is given by equation S3, in which scale(peak) is a scale factor, q_0 is the peak position in q, and B is the half-width at half-maximum.

$$I_{peak} = \frac{scale(peak)}{\left(1 + \left(\frac{q - q_0}{B}\right)\right)} \quad \text{(S3)}$$

For the SAXS fitting, ρ_1, ρ_2, and ρ_3 were set to 8.7×10^{-6} Å^{-2}, 11.2×10^{-6} Å^{-2}, 7.2×10^{-6} Å^{-2}, respectively, which were estimated using SLD calculator tool of SasView software. ρ_0 (ρ_{core}) was set to 7.5×10^{-6} Å^{-2}, which was calculated for a volume-fraction-weighted sum of the ρ of MCH and toluene. The obtained parameters for toroids are shown below. The "*" denotes parameters were held fixed to values.

Table S1. Parameters obtained from fitting the SAXS profile of toroids.

core radius (nm)	core length (nm)	shell1 thickness (nm)	shell2 thickness (nm)
3.6808 ± 0.0090423	5.1966 ± 0.012	0.94358 ± 0.014437	2.1819 ± 0.011935

shell3 thickness (nm)	peak position (nm^{-1})	peak hwhm (nm^{-1})
1.2767 ± 0.026969	2.3*	0.0042635*

Estimation of the fraction of toroid *n*-mers:

For each sample, we measured thickness of toroids using cross-sectional analysis mode in Nanoscope Analysis 3.00, and then assigned the number of stacked toroids on the basis of these thickness profiles. Thereby, the numbers of toroid monomer, toroid dimer, and toroid oligomer were counted in 1.0 × 1.0 μm² AFM images using the Point Tool in ImageJ. More than 2500 toroids were counted for each condition. The fraction of toroid *n*-mer was calculated using following the equation S4.

$$\text{The fraction of toroid } n\text{-mer} = \frac{\text{number of toroid } n\text{-mer} \times n}{\text{total number of toroids}} \qquad \text{(S4)}$$

Table S2. The fraction of toroid *n*-mer

Conc. [μM]	14.8	30.0	50.4	120	59.3	29.8	14.7	7.18
Toroid monomer	0.53	0.35	0.15	0.13	0.15	0.14	0.18	0.25
Toroid dimer	0.47	0.65	0.80	0.85	0.83	0.85	0.82	0.75
Toroid oligomer	0.00	0.00	0.05	0.02	0.02	0.01	0.00	0.00

2. Synthesis and Characterization

Compound **2** was synthesized by the following procedure as shown in Scheme S1. Synthesis of **3, 5** and **7** were reported previously.[S8–S10]

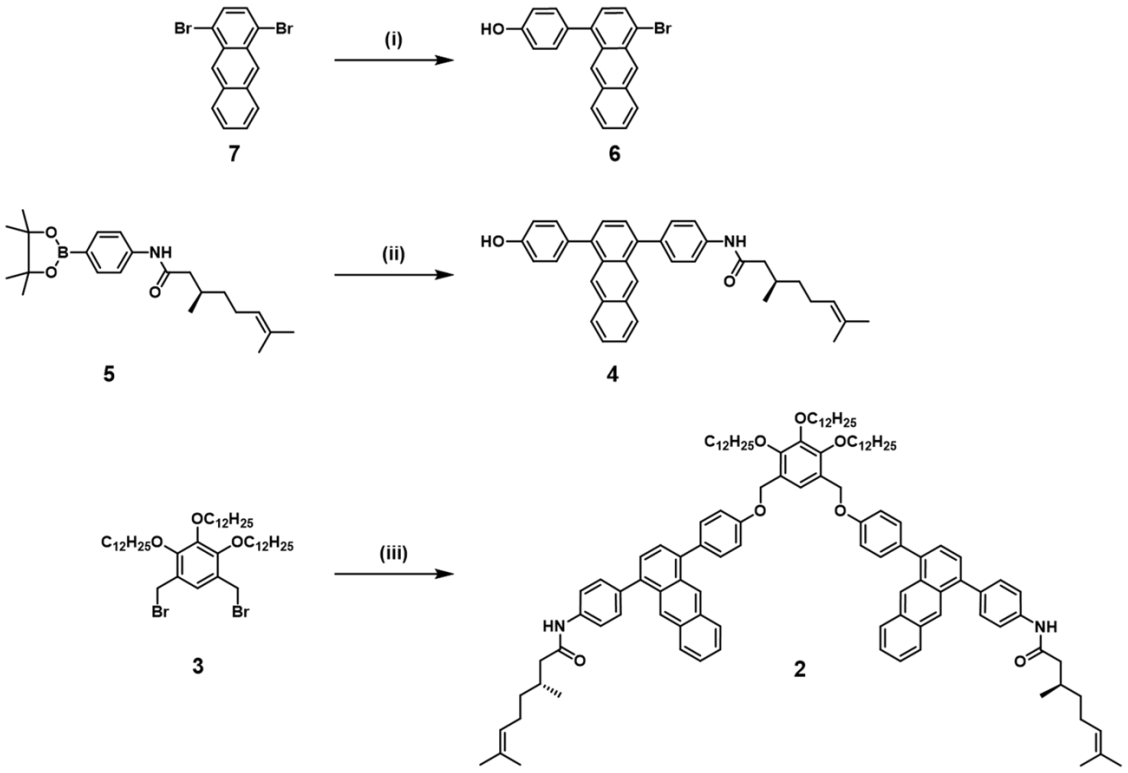

Scheme S1. Synthesis of **2**. Reagents and conditions: (i and ii) $Pd(PPh_3)_4$, K_2CO_3, THF/water, 70 °C; (iii) K_2CO_3, DMF, 70 °C.

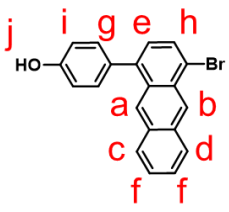

Synthesis and characterization of compound 6: A three-neck round-bottom flask was charged with compound **7** (603 mg, 1.79 mmol), 4-hydroxyphenylboronic acid (259 mg, 1.88 mmol), K_2CO_3 (736 mg, 5.33 mmol), and $Pd(PPh_3)_4$ (171 mg, 0.148 mmol) under N_2 atmosphere. A degassed mixture of THF (40 mL) and water (10 mL) was added, and the resulting mixture was stirred at 70 °C under N_2 atmosphere for 13 h. After cooling to room temperature, the reaction mixture was neutralized with aq. HCl (2 M). The resulting solution was passed through a small pad of Celite®. The filtrate was diluted with EtOAc, and the resulting solution was washed with H_2O and brine. The organic layer was separated, dried over Na_2SO_4 and then evaporated to dryness under a reduced pressure. The crude product was purified by column chromatography over silica gel (eluent: EtOAc:*n*-hexane = 1:3, v/v) and further

purified by filtration (eluent: *n*-hexane) to give **6** as a yellow solid (253 mg, 40% yield). ^{1}H NMR (500 MHz, $CDCl_3$, 293 K, see Chart S1): δ = 8.89 (s, 1H, AnthH_a), 8.45 (s, 1H, AnthH_b), 8.10 (d, J = 8.27 Hz, 1H, AnthH_c), 7.90 (d, J = 8.34 Hz, 1H, AnthH_d), 7.83 (d, J = 7.39 Hz, 1H, AnthH_e), 7.53–7.47 (m, 2H, AnthH_f), 7.43 (d, J = 8.58 Hz, 2H. PhH_g), 7.20 (d, J = 7.39 Hz, 1H, AnthH_h), 7.02 (d, J = 8.58 Hz, 2H, PhH_i), 4.92 (s, 1H, PhOH_j). ^{13}C NMR (126 MHz, $CDCl_3$, 20 °C, see Chart S2): δ = 155.27, 140.10, 132.72, 132.04, 131.91, 131.37, 131.30, 130.20, 128.93, 128.39, 128.30, 126.61, 126.31, 126.14, 126.00, 122.09, 115.40. HRMS (ESI): *m*/*z* calcd for $C_{20}H_{12}OBr$ 347.0077 $[M+H]^+$, found 347.0072.

Synthesis and characterization of compound 4: A three-neck round-bottom flask was charged with compound **6** (214 mg, 0.613 mmol), **5** (351 mg, 0.945 mmol), K_2CO_3 (250 mg, 1.81 mmol), and $Pd(PPh_3)_4$ (92 mg, 0.0796 mmol) under N_2 atmosphere. A degassed mixture of THF (20 mL) and degassed water (5 mL) was added, and the resulting mixture was stirred at 70 °C under N_2 atmosphere for 16 h. After cooling to room temperature, the reaction mixture was neutralized with aq. HCl (2 M). The resulting solution was passed through a small pad of Celite®. The filtrate was diluted with EtOAc, and the resulting solution was washed with H_2O and brine. The organic layer was separated, dried over Na_2SO_4 and then evaporated to dryness under a reduced pressure. The crude product was purified by column chromatography over silica gel (eluent: EtOAc:*n*-hexane = 1:3, v/v) to give **4** as an orange solid (223 mg, 69% yield). ^{1}H NMR (500 MHz, $CDCl_3$, 293 K, see Chart S3): δ = 8.52 (s, 2H, AnthH_a), 7.89–7.87 (m, 2H, AnthH_b), 7.72 (d, J = 8.44 Hz, 2H, PhH_c), 7.59 (d, J = 8.44 Hz, 2H, PhH_d), 7.49 (d, J = 8.48 Hz, 2H, PhH_e), 7.42–7.34 (m, 4H, AnthH_f), 7.30 (s, 1H, PhNH_gCO), 7.04 (d, J = 8.53 Hz, 2H, PhH_h), 5.25 (1H, s, PhOH_i), 5.15 (t, J = 7.09 Hz, 1H, CH_j=C(CH_3)$_2$), 2.49–2.46 (m, 1H, CH_k), 2.24–2.04 (m, 4H, C$H_{l,m}$), 1.71 (s, 3H, CH_n), 1.64 (s, 3H, CH_o), 1.55–1.29 (m, 2H, CH_p), 1.08 (d, J = 6.46 Hz, 3H, CH_q). ^{13}C NMR (126 MHz, $CDCl_3$, 20 °C, see Chart S4): δ = 171.32, 155.33, 139.50, 138.84, 137.17, 137.04, 133.29, 131.79, 131.42, 131.37, 131.34, 130.83, 130.63, 128.33, 128.31, 125.86, 125.69, 125.58, 125.54, 125.39, 125.18, 124.26, 120.09, 115.42, 45.69, 36.95, 30.74, 25.80, 25.56, 19.68, 17.77. HRMS (ESI): *m*/*z* calcd for $C_{36}H_{36}NO_2$ 514.2741 $[M+H]^+$, found 514.2737.

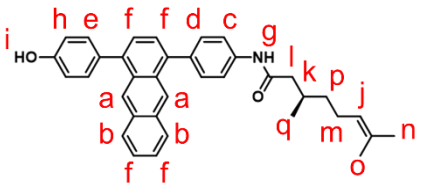

Synthesis and characterization of compound 2: Compound **4** (100 mg, 195 μmol), **3** (65 mg, 80 μmol), and K_2CO_3 (68 mg, 0.49 mmol) were dissolved in 3 mL of dry DMF, and the mixture was stirred for at 70 °C under N_2 atmosphere for 14 h. After cooling to room temperature, the reaction mixture was diluted with EtOAc, and the resulting solution was washed with H_2O and brine. The organic layer was separated, dried over Na_2SO_4 and then evaporated to dryness under a reduced pressure. The crude product was purified by column chromatography over silica gel (eluent: EtOAc:*n*-hexane = 1:4, v/v) and further purified by GPC (eluent: $CHCl_3$) to give compound **2** as a yellow solid (32 mg, 24% yield). ^{1}H NMR (500 MHz, $CDCl_3$, 293 K, see Chart S5): δ = 8.54 (s, 2H, AnthH_a), 8.50 (s, 2H, AnthH_b), 7.88–7.86 (m, 4H, AnthH_c), 7.70 (d, J = 8.39 Hz, 4H, PhH_d), 7.56–7.52 (m, 8H, PhH_e), 7.46 (s, 1H, PhH_f), 7.40–7.31 (m, 10H, AnthH_g and PhNH_gCO), 7.18 (d, J = 8.53 Hz, 4H, PhH_h), 5.23 (s, 4H, PhCH_i), 5.15 (t, J = 7.16 Hz, 2H, CH_j=C(CH$_3$)$_2$), 4.16 (t, J = 6.58 Hz, 4H, CH_k), 4.08 (t, J = 6.67 Hz, 2H, CH_l), 2.50–2.46 (m, 2H, CH_m), 2.25–2.06 (m, 8H, C$H_{n,o}$), 1.83–1.79 (m, 6H, CH_p), 1.71 (s, 6H, CH_q), 1.65 (s, 6H, CH_r), 1.53–1.46 (m, 6H, CH_s), 1.36–1.20 (m, 52H, CH_t), 1.09 (d, J = 6.37 Hz, 6H, CH_u), 0.89–0.82 (m, 9H, CH_v). ^{13}C NMR (126 MHz, $CDCl_3$, 20 °C, see Chart S4): δ = 171.11, 158.44, 151.86, 145.90, 139.47, 138.82, 137.14, 137.03, 133.42, 131.75, 131.36, 131.33, 131.25, 130.80, 130.63, 128.34, 128.30, 126.04, 125.82, 125.68, 125.55, 125.50, 125.40, 125.19, 124.29, 120.04, 114.80, 74.36, 73.79, 65.56, 45.68, 36.97, 31.97, 31.92, 30.72, 30.53, 30.47, 29.78, 29.77, 29.74, 29.69, 29.65, 29.43, 29.38, 26.27, 26.24, 25.80, 25.57, 22.74, 22.70, 19.69, 17.77, 14.17, 14.14. HRMS (ESI): *m*/*z* calcd for $C_{116}H_{149}O_7N_2$ 1682.1359 $[M+H]^+$, found 1682.1362.

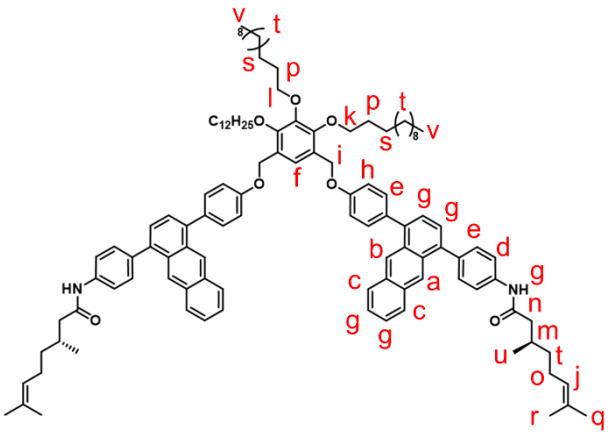

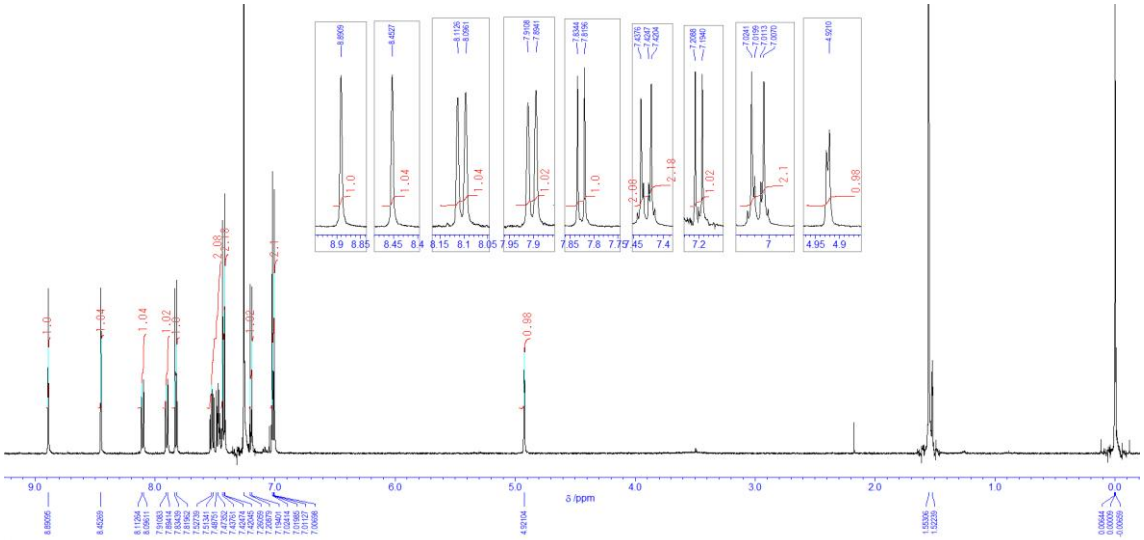

Chart S1 ^{1}H NMR spectrum of **6** in $CDCl_3$ at 293 K.

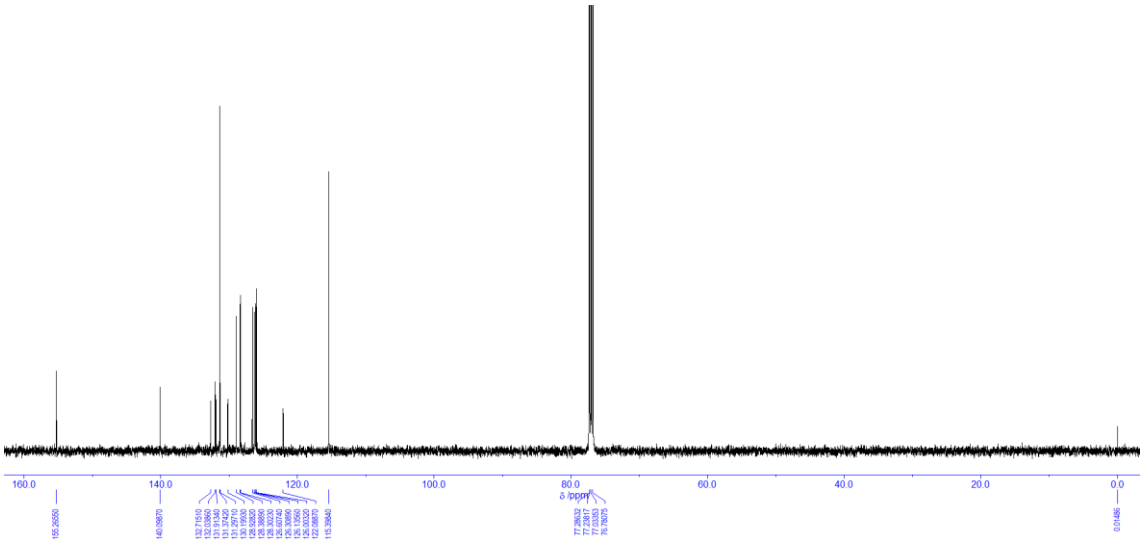

Chart S2 ^{13}C NMR spectrum of **6** in $CDCl_3$ at 293 K.

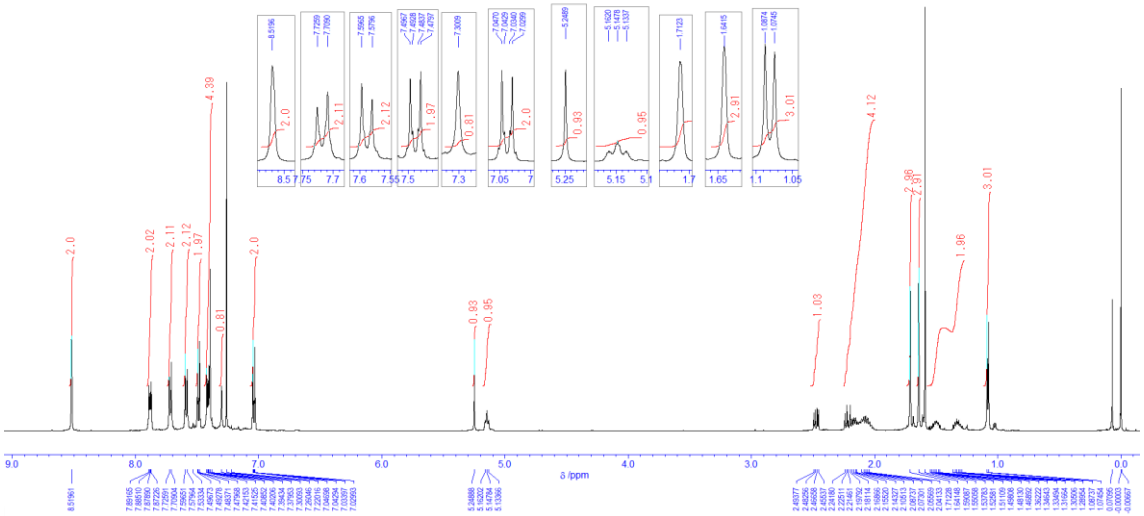

Chart S3 ^{1}H NMR spectrum of **4** in $CDCl_3$ at 293 K.

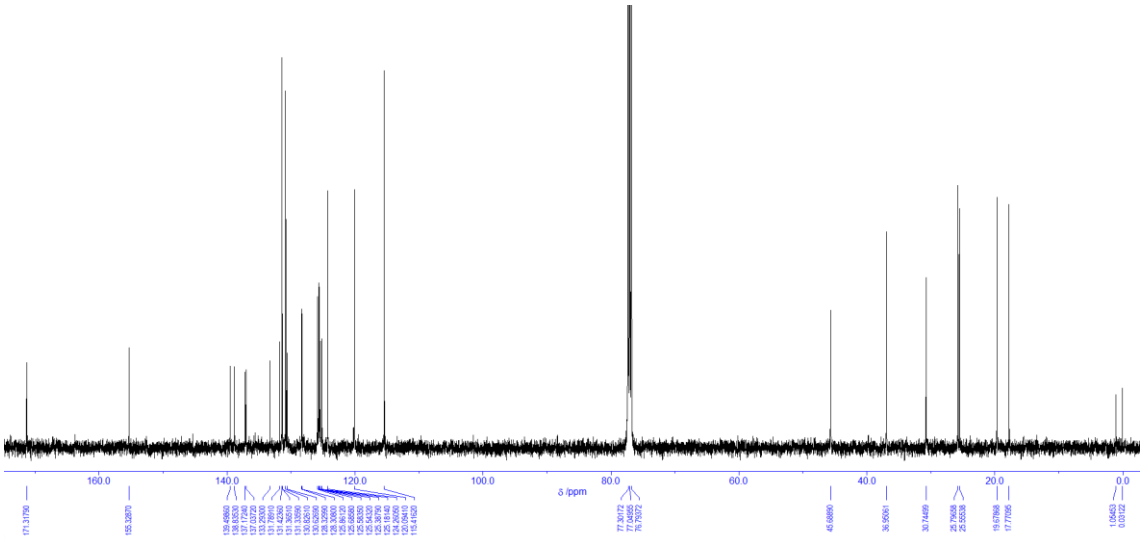

Chart S4 ^{13}C NMR spectrum of **4** in $CDCl_3$ at 293 K.

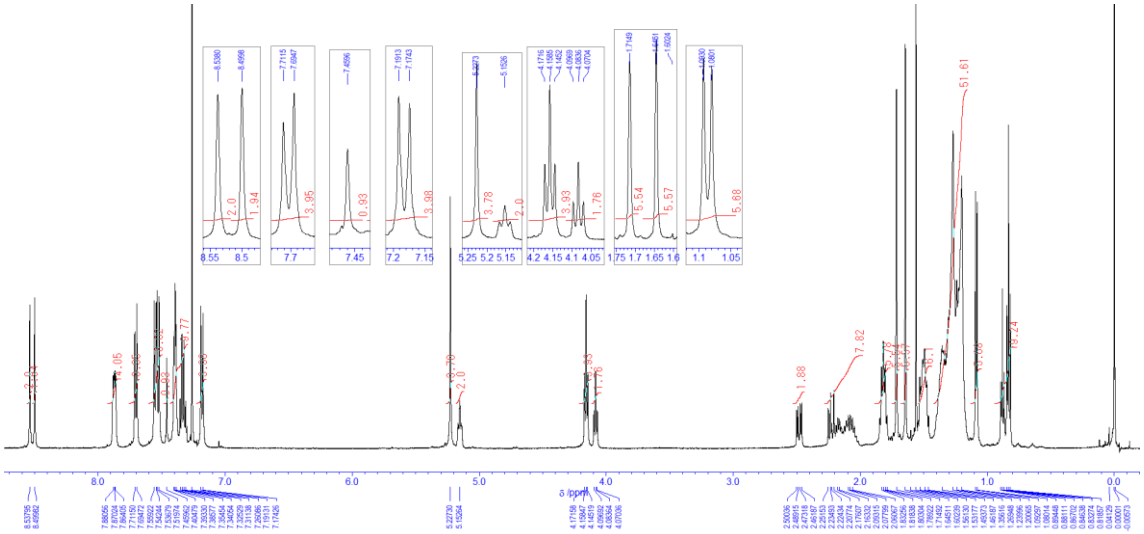

Chart S5 ^{1}H NMR spectrum of **2** in $CDCl_3$ at 293 K.

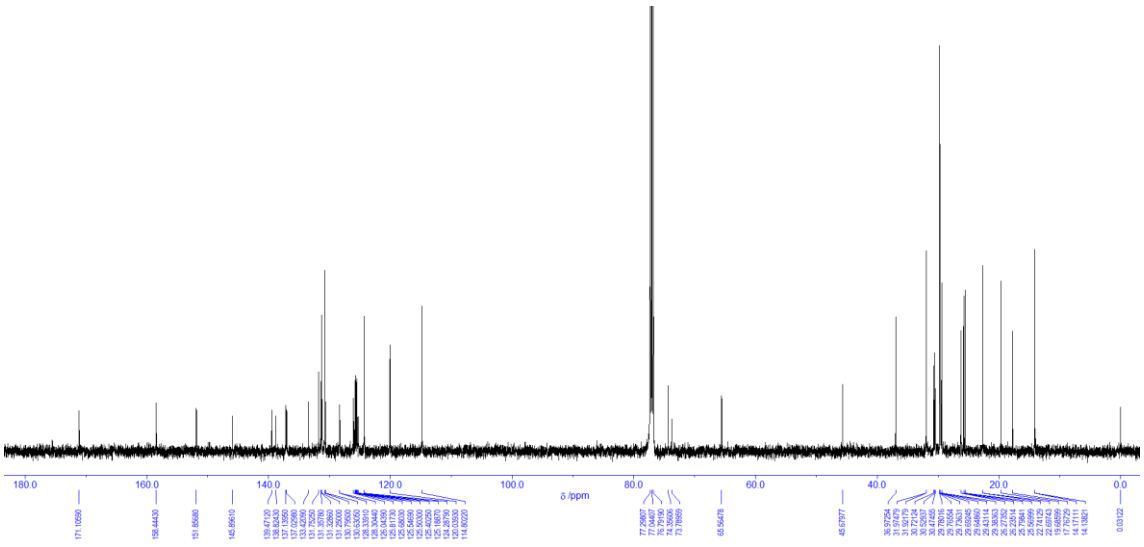

Chart S6 ^{13}C NMR spectrum of **2** in $CDCl_3$ at 293 K.

3. Supporting Figures

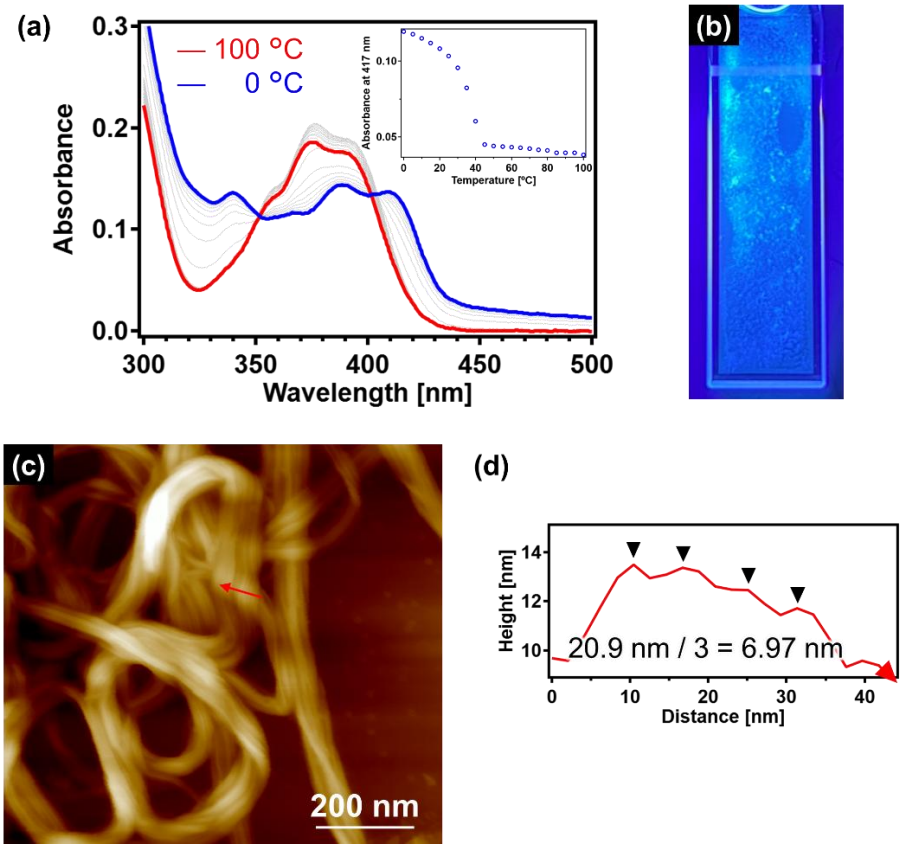

Fig. S1 (a) UV/Vis absorption spectra of **2** (c = 100 μM) in MCH containing 10% (v/v) toluene upon cooling from 100 °C (red line) to 0 °C (blue line) at a rate of 1 °C min^{-1}. The intermediate spectra were measured every 5 °C. Inset: cooling profiles obtained by plotting the change in absorption at 417 nm as a function of temperature. (b) Photograph of a precipitated solution of **2** after cooling under 365 nm UV light illumination. (c) AFM image of the precipitated fibers of **2** (c = 100 μM). (d) AFM cross-sectional analysis of fibers along the red arrow in (c).

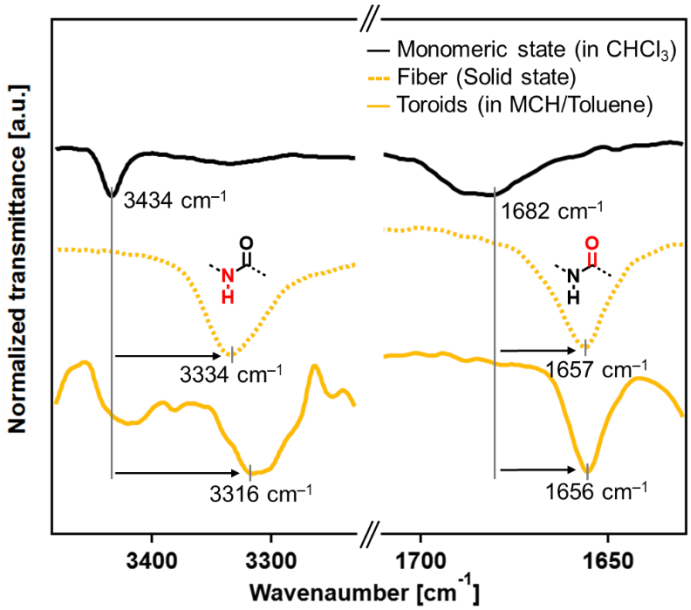

Fig. S2 FT-IR spectra of monomeric **2** in $CHCl_3$ (c = 300 μM, black solid line), fibers of **2** (solid state, yellow dotted line) and toroids of **2** in MCH containing 10% (v/v) toluene (c = 340 μM, yellow solid line). The toroid solution was prepared by passing the entire suspension through a membrane filter, and then concentrating the filtrate. Under these concentrated conditions, the spectrum of the toroid sample predominantly reflects toroid dimers (see Fig. 3a and 4a for details).

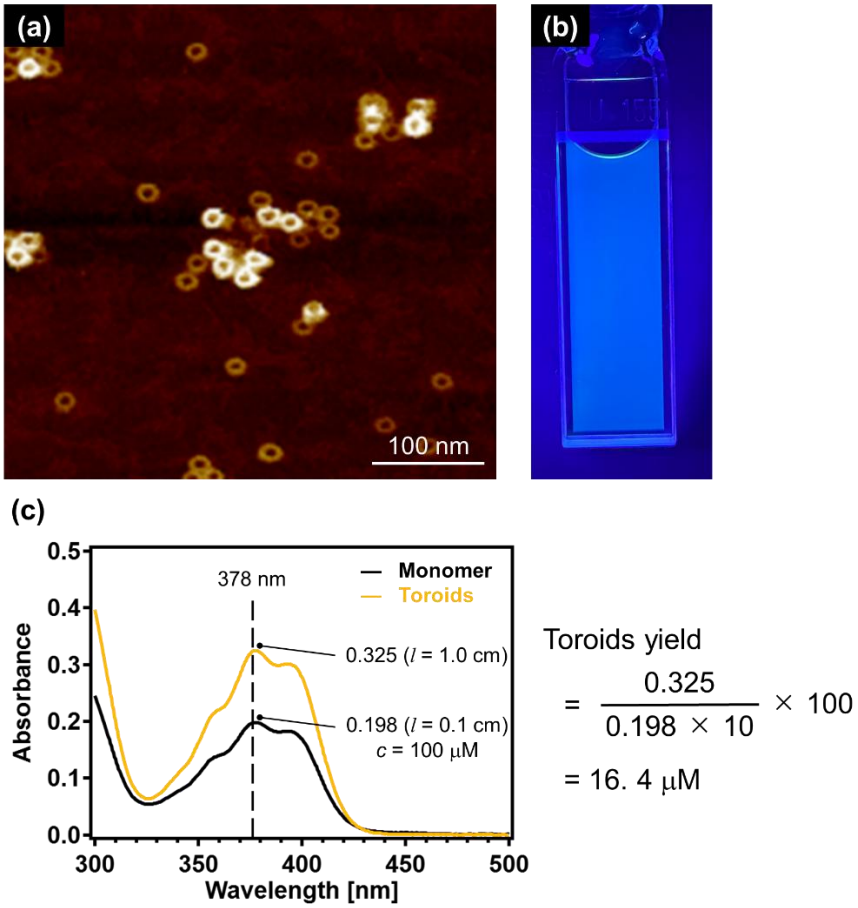

Fig. S3 (a) AFM image of the filtrate of **2** in MCH containing 10% (v/v) toluene. (b) Photograph of the filtrate under 365 nm UV light illumination. (c) UV/Vis absorption spectra of a monomer solution of **2** (c = 100 μM) in $CHCl_3$ at 50 °C (black line) and the filtrate evaporated and re-dissolved in $CHCl_3$ at 50 °C (yellow line).

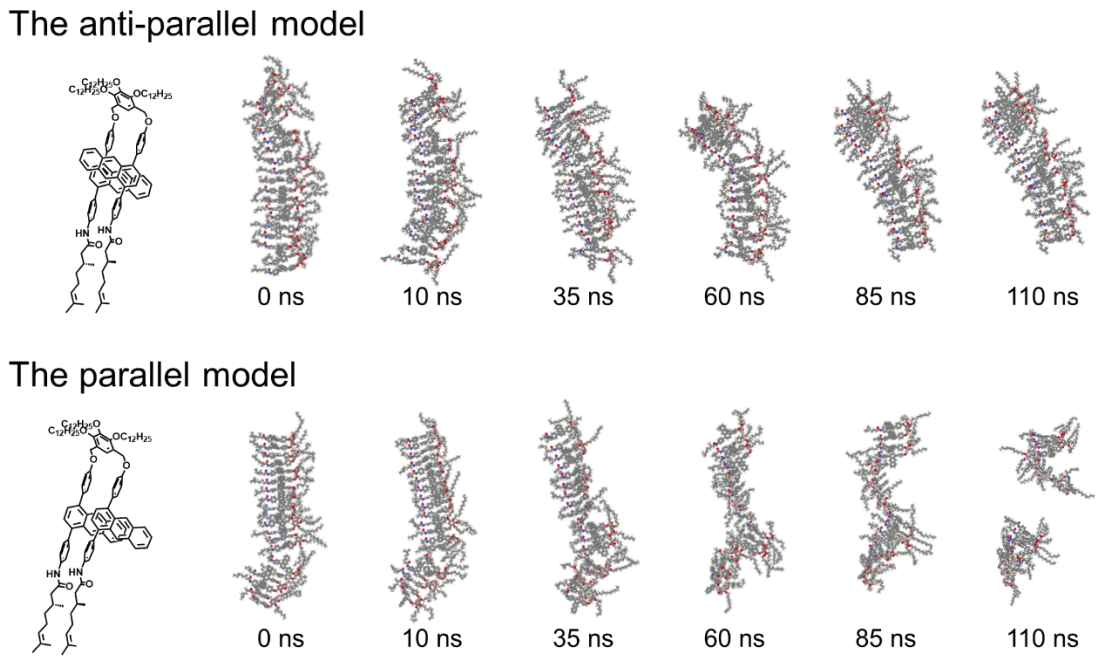

Fig. S4 Molecular structures and snapshots of the equilibrated fiber of **2** obtained during the production run (0–110 ns) of the MD simulation for the anti-parallel and parallel models.

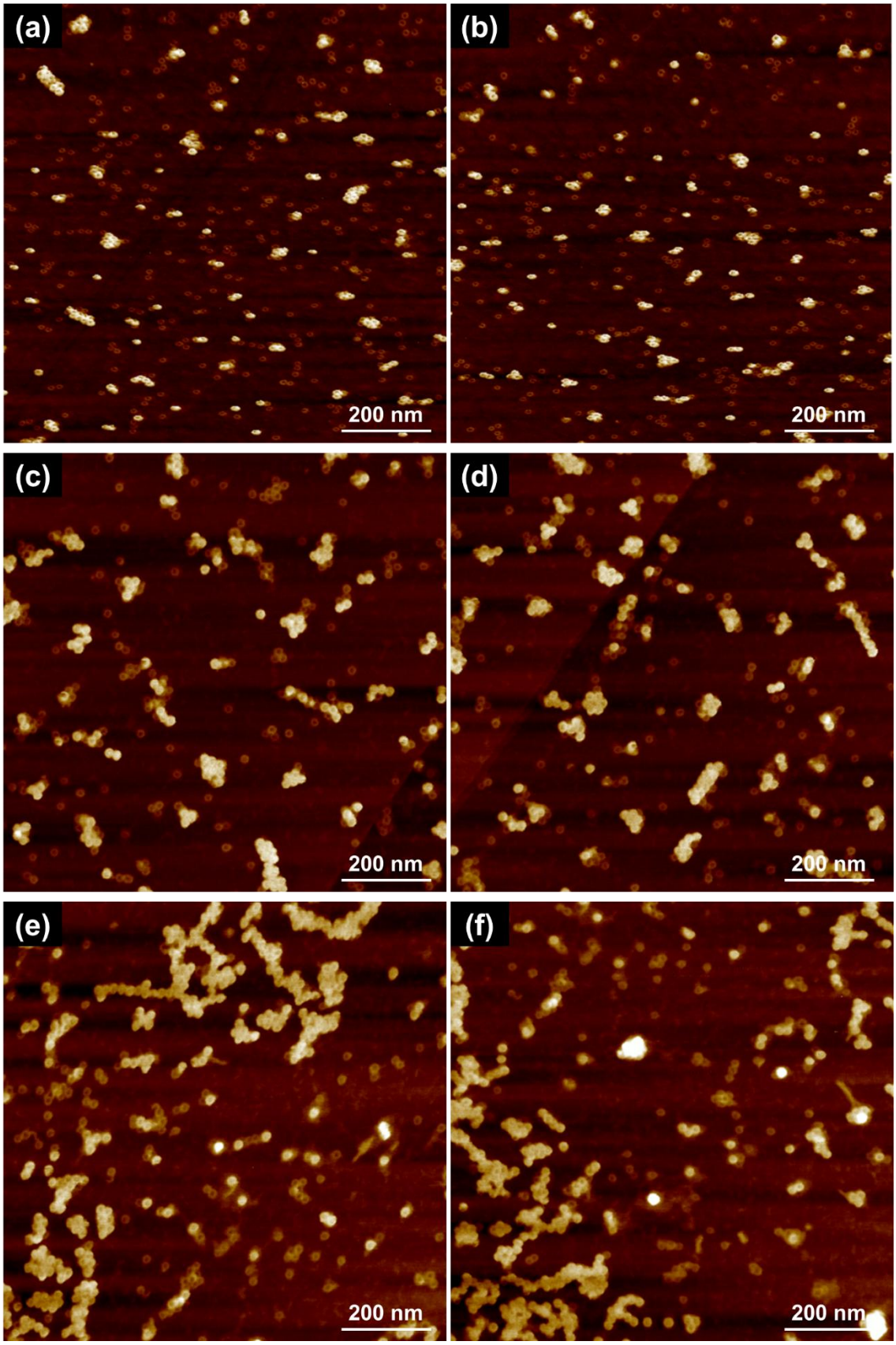
(a)
200 nm
(b)
200 nm
(c)
200 nm
(d)
200 nm
(e)
200 nm
(f)
200 nm

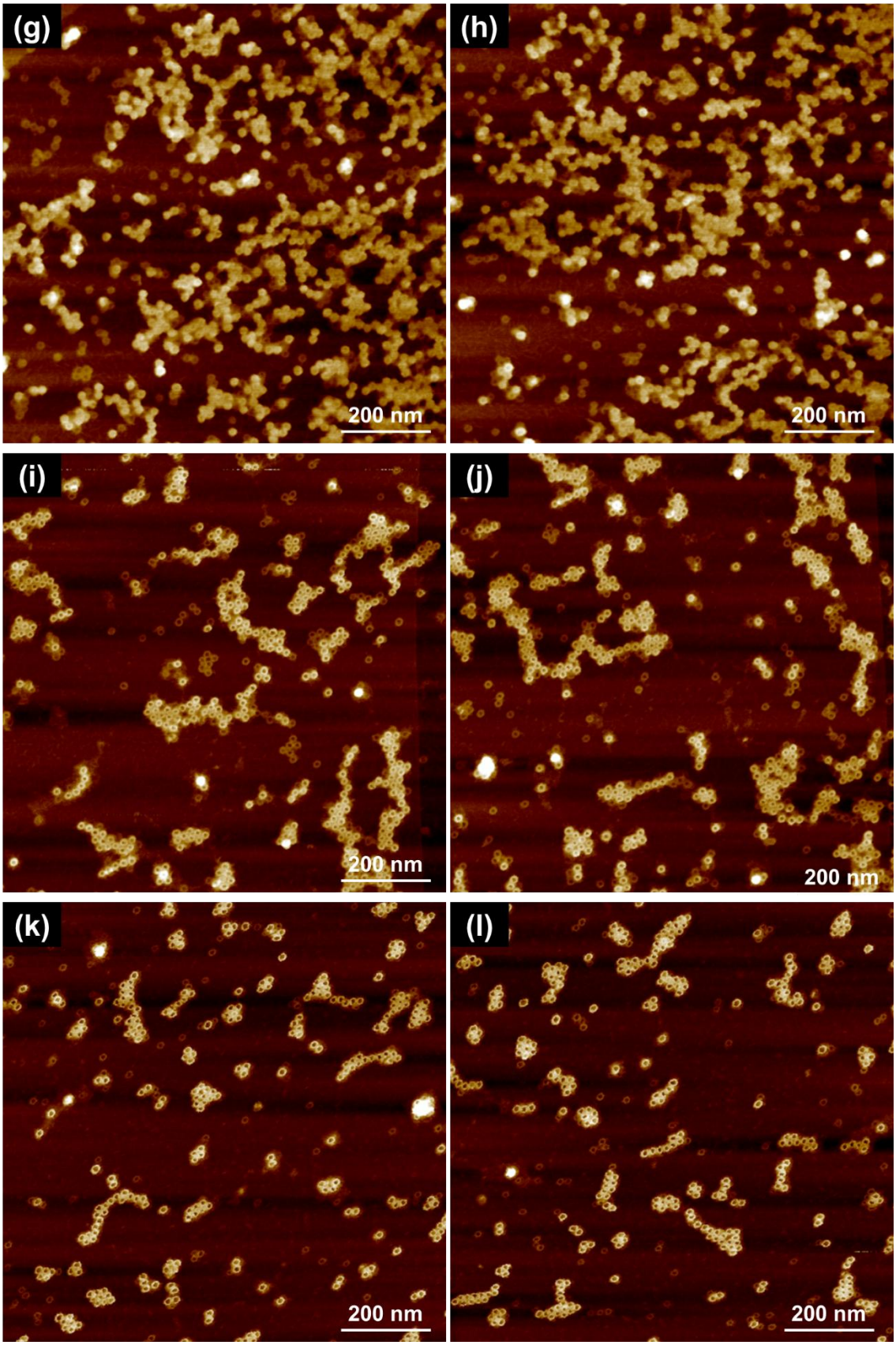
(g)
200 nm
(h)
200 nm
(i)
200 nm
(j)
200 nm
(k)
200 nm
(l)
200 nm

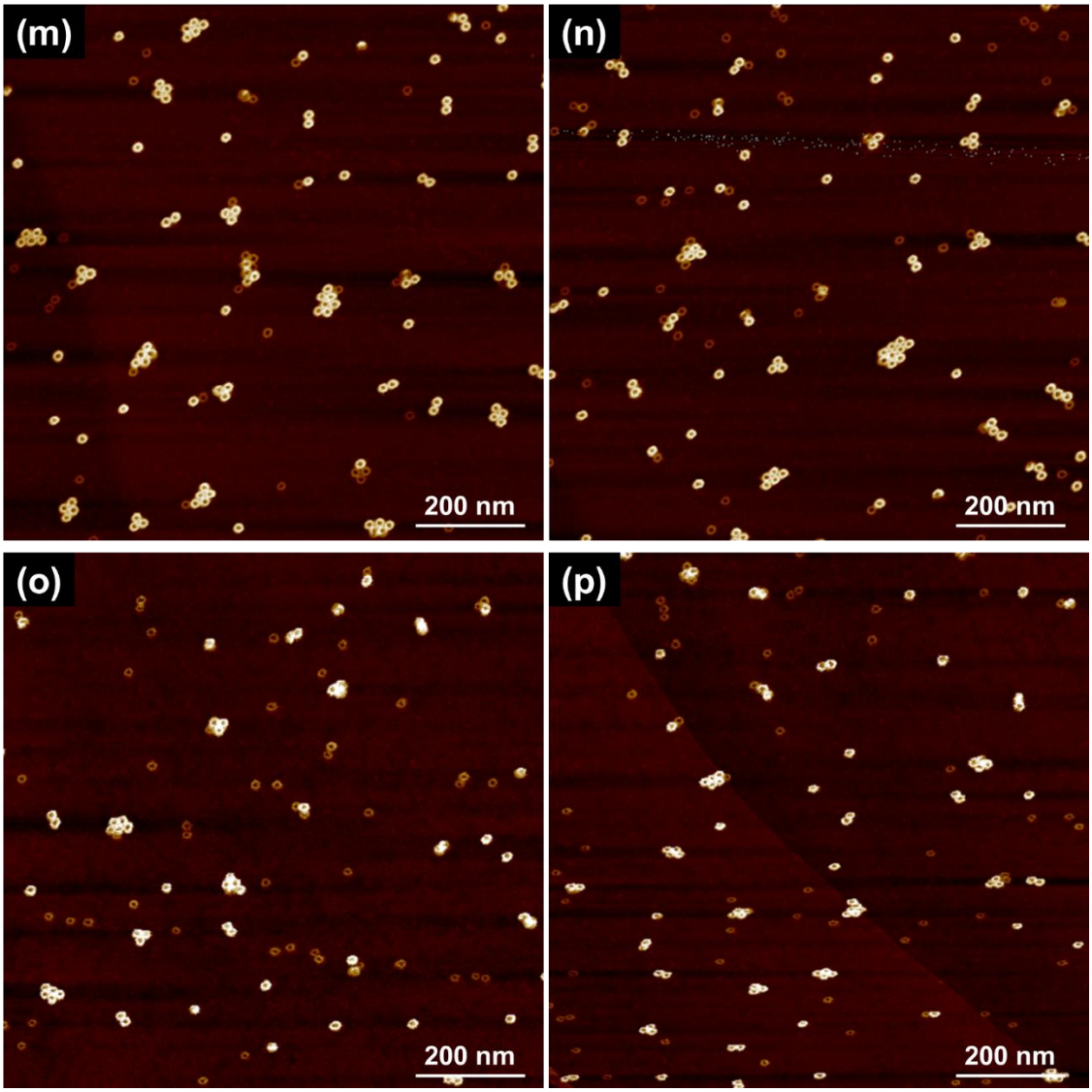

Fig. S5 (a–p) AFM images of toroids of **2** (c = 14.8 μM) in MCH containing 10% (v/v) toluene upon concentration to c = (a and b) 14.8 μM, (c and d) 30.0 μM, (e and f) 50.4 μM and (g and h) 120 μM, and upon subsequent dilution to c = (i and j) 59.3 μM, (k and l) 29.8 μM, (m and n) 14.7 μM and (o and p) 7.18 μM.

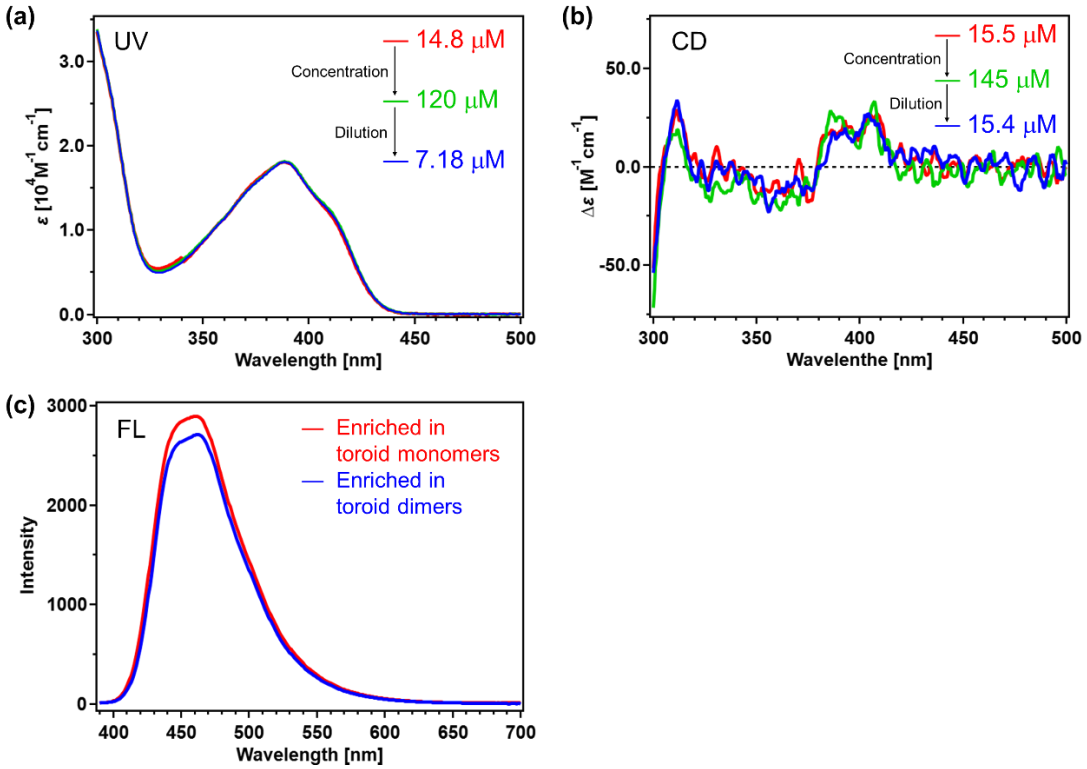

Fig. S6 (a) UV/Vis absorption spectra of toroids of **2** (c = 14.8 μM, red line) in MCH containing 10% (v/v) toluene upon concentration to c = 120 μM (green line), and upon subsequent dilution to c = 7.18 μM (blue line). (b) Circular dichroism spectra of toroids of **2** (c = 15.5 μM, red line) in MCH containing 10% (v/v) toluene upon concentration to c = 145 μM (green line), and upon subsequent dilution to c = 15.4 μM (blue line). (c) Fluorescence spectra of toroids in MCH containing 10% (v/v) toluene. Red line shows the enriched toroid monomer solution (c = 12.6 μM), and blue line shows the enriched toroid dimer solution (c = 13.8 μM) after concentration of the above solution, followed by dilution.

4. Supporting References

S1 M. Abraham, A. Alekseenko, B. Andrews, V. Basov, P. Bauer, H. Bird, E. Briand, A. Brown, M. Doijade, G. Fiorin, S. Fleischmann, S. Gorelov, G. Gouaillardet, A. Gray, M. E. Irrgang, F. Jalalypour, P. Johansson, C. Kutzner, G. Łazarski, J. A. Lemkul, M. Lundborg, P. Merz, V. Miletić, D. Morozov, L. Müllender, J. Nabet, S. Páll, A. Pasquadibisceglie, M. Pellegrino, N. Piasentin, D. Rapetti, M. U. Sadiq, H. Santuz, R. Schulz, M. Shirts, T. Shugaeva, A. Shvetsov, P. Turner, A. Villa, S. Wingbermühle, B. Hess, E. Lindahl, "GROMACS 2025.4 Manual" 2025, DOI 10.5281/ZENODO.17671776.

S2 J. Wang, R. M. Wolf, J. W. Caldwell, P. A. Kollman and D. A. Case, J. Comput. Chem., 2004, 25, 1157–1174.

S3 M. J. Frisch, G. W. Trucks, H. B. Schlegel, G. E. Scuseria, M. A. Robb, J. R. Cheeseman, G. Scalmani, V. Barone, G. A. Petersson, H. Nakatsuji, X. Li, M. Caricato, A. V. Marenich, J. Bloino, B. G. Janesko, R. Gomperts, B. Mennucci, H. P. Hratchian, J. V. Ortiz, A. F. Izmaylov, J. L. Sonnenberg, D. Williams-Young, F. Ding, F. Lipparini, F. Egidi, J. Goings, B. Peng, A. Petrone, T. Henderson, D. Ranasinghe, V. G. Zakrzewski, J. Gao, N. Rega, G. Zheng, W. Liang, M. Hada, M. Ehara, K. Toyota, R. Fukuda, J. Hasegawa, M. Ishida, T. Nakajima, Y. Honda, O. Kitao, H. Nakai, T. Vreven, K. Throssell, J. A. Montgomery Jr., J. E. Peralta, F. Ogliaro, M. J. Bearpark, J. J. Heyd, E. N. Brothers, K. N. Kudin, V. N. Staroverov, T. A. Keith, R. Kobayashi, J. Normand, K. Raghavachari, A. P. Rendell, J. C. Burant, S. S. Iyengar, J. Tomasi, M. Cossi, J. M. Millam, M. Klene, C. Adamo, R. Cammi, J. W. Ochterski, R. L. Martin, K. Morokuma, O. Farkas, J. B. Foresman and D. J. Fox, Gaussian 16 C02.

S4 B. Hess, H. Bekker, H. J. C. Berendsen and J. G. E. M. Fraaije, *J. Comput. Chem.*, 1997, **18**, 1463–1472.

S5 N. Shimizu, K. Yatabe, Y. Nagatani, S. Saijyo, T. Kosuge and N. Igarashi, *AIP Conf. Proc.*, 2016, **1741**, 050017.

S6 core_multishell_cylinder — SasView 5.0.4 documentation, https://www.sasview.org/downloads/core_multi_shell_cylinder_docs.pdf, (accessed Dec 2025).

S7 peak_lorentz — SasView 6.0.1 documentation, https://www.sasview.org/docs/user/models/peak_lorentz.html, (accessed Dec 2025).

S8 T. Aizawa, H. Arima, S. Mihara, T. Ueno, S. Yoshii, T. Saito, H. Itabashi, S. Datta, H. Hanayama, A. Sakamoto, R. Shimada, S. E. Rogers, M. J. Hollamby, T. Kajitani, Y. Ishii, G. Watanabe, K. Harano, T. Matsumoto, N. Pathoor, M. Vacha, H. Sotome and S. Yagai, DOI:10.26434/chemrxiv-2025-d7n17.

S9 M. Feofanov, V. Akhmetov, D. I. Sharapa and K. Amsharov, *Org. Lett.*, 2020, **22**, 1698–1702.

S10 S. Yao, U. Beginn, T. Gress, M. Lysetska and F. Würthner, *J. Am. Chem. Soc.*, 2004, **126**, 8336–8348.